University of Massachusetts - Amherst

From the SelectedWorks of David Ostendorf

January 2007

Water hammer dissipation in pneumatic slug tests

Contact Author

Start Your Own SelectedWorks

Notify Me of New Work

Available at: http://works.bepress.com/david_ostendorf1/3

Water hammer dissipation in pneumatic slug tests

David W. Ostendorf,[1] Don J. DeGroot,[1] and Philip J. Dunaj[1]

Received 16 December 2005; revised 31 August 2006; accepted 2 October 2006; published 14 February 2007.

[1] We model and measure the dissipation of water hammer induced by well casing and water elasticity with rapid valve opening at the start of a pneumatic slug test. The higher-frequency water hammer can obscure slower, aquifer-controlled, underdamped oscillations of the rigid water column, so a quantitative description of the elastic motion improves the ability of a slug test to calibrate the aquifer permeability k. Internal friction attenuates the water hammer, subject to a known headspace pressure at the air/water interface and equilibrium pressure at the top of the well screen. An analytical elastic solution is presented and matched to an existing rigid motion analysis, with matching predicated on k exceeding 7×10^{-14} m^2 and appreciable water hammer dissipation during the first cycle of the slug test. The model is accurately calibrated with data from underdamped slug tests in a PVC monitoring well in the Plymouth-Carver Aquifer. The calibrated casing elasticity value suggests that effective lateral soil stress appreciably stiffened the casing.

Citation: Ostendorf, D. W., D. J. DeGroot, and P. J. Dunaj (2007), Water hammer dissipation in pneumatic slug tests, *Water Resour. Res.*, *43*, W02413, doi:10.1029/2005WR004817.

1. Introduction

[2] We study ≈10 Hz frequency elastic disturbances at the start of pneumatic slug tests. This water hammer, which is governed by casing and water elasticity, is induced by rapid opening of the valve that depressurizes the headspace. The slug tests eventually induce rigid motion controlled by the aquifer permeability, and a long-established literature [*Hvorslev*, 1951; *Bouwer and Rice*, 1976] estimates the property for damped slug tests in moderately permeable soil. Underdamped slug tests exhibit a periodic, aquifer controlled response at ~0.1 Hz frequency for deeper wells in more permeable formations, and the theory of *van der Kamp* [1976] and *Springer and Gelhar* [1991] describes the rigid motion. *Proesser* [1981] and *Zemansky and McElwee* [2005] qualitatively document the higher-frequency disturbances that obscure the transient response of the aquifer immediately after the opening of the valve. *Zurbuchen et al.* [2002] and *Ostendorf et al.* [2005] offer more quantitative accounts of the phenomenon, and suggest that elasticity plays a role in explaining it.

[3] Our present research pursues the matter in the water column, with temporally resolved data and theory. The data feature a kHz acquisition system. The water hammer theory is linear and analytical, and illustrated by simulations. The water hammer frequency is assumed rapid enough to establish a linear pressure gradient in the column that varies from a screen section value in equilibrium with the surrounding groundwater to gauge pressure at the suppressed air/water interface. The linear pressure gradient serves as an initial condition for the slower rigid column response modeled by the conventional slug test theory. The water hammer theory and rigid column match, and may be superimposed so long as the former frequency is much faster than that of the latter and the water hammer dissipation is rapid. This is fortunately the case for permeable aquifers, which are most likely to be tested pneumatically. A calibration at the Plymouth-Carver Aquifer demonstrates the validity and use of the model to interpret field data with plausible parameter values.

2. Theory

2.1. Governing Equation and Initial and Boundary Conditions

[4] The conservation of water mass equation balances flux and storage in a monitoring well, with the latter released by elastic well casing and compressible fluid

$$\frac{\partial(\rho A)}{\partial t} + \rho A \frac{\partial w}{\partial z} = 0 \tag{1a}$$

$$\frac{dA}{A} = \frac{Ddp}{bp_C} \tag{1b}$$

$$\frac{d\rho}{\rho} = \frac{dp}{p_W} \tag{1c}$$

with water density ρ, time t, elevation z above the screen section, and velocity w (Figure 1). Large gauge pressure p changes induce the elastic response and create dominant velocity changes in the second term of equation (1a). *Streeter et al.* [1998] relate the change dA in cross sectional area to the elasticity p_C, inner diameter D, and thickness b of the casing in equation (1b). The compressibility p_W of water governs the contribution of the fluid to storage change in

[1]Civil and Environmental Engineering Department, University of Massachusetts, Amherst, Massachusetts, USA.

Copyright 2007 by the American Geophysical Union.
0043-1397/07/2005WR004817

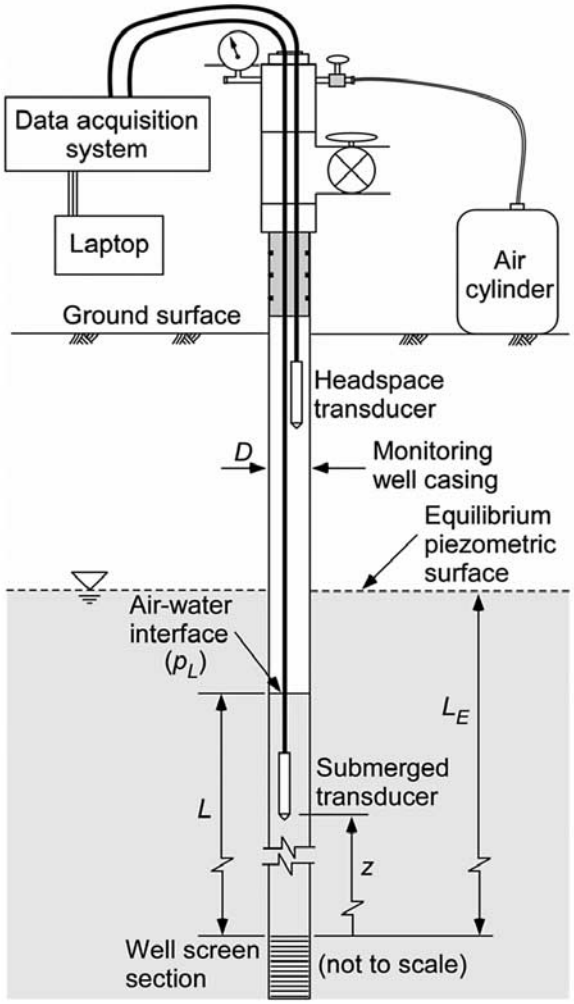

Figure 1. Pneumatic slug tester [*Ostendorf et al.*, 2005] and definition sketch, showing suppressed air-water interface (elevation L) at the start of the test.

equation (1c). The chain rule reduces equations (1) to a linearized water mass equation

$$\frac{\partial p}{\partial t} + \left(\frac{D}{bp_C} + \frac{1}{p_W}\right)^{-1} \frac{\partial w}{\partial z} = 0 \tag{2a}$$

$$w = -\left(\frac{D}{bp_C} + \frac{1}{p_W}\right) \int \frac{\partial p}{\partial t} dz \tag{2b}$$

Equation (2b) expresses velocity in terms of pressure fluctuations. A similar equation governs acoustic waves through the headspace, with atmospheric pressure replacing the inverse pressure term in front of the integral. Since the atmospheric pressure is four orders of magnitude smaller than the casing or water elasticity, the air speed is much faster than the water speed. The wall shear stress from this rapid air velocity dissipates the acoustic waves, while internal friction caused by imperfect elasticity is assumed to dissipate the water hammer.

[5] The conservation of vertical momentum accordingly balances acceleration, internal friction, weight, and a pressure gradient in the casing

$$\frac{\partial w}{\partial t} = -\Gamma w - g - \frac{1}{\rho}\frac{\partial p}{\partial z} \tag{3}$$

with gravitational acceleration g. We ignore the momentum flux [*Streeter et al.*, 1998]. The damping coefficient Γ relates the internal friction to velocity, as is common in solid mechanics [*Weaver et al.*, 1990]. This parameter reflects imperfect elasticity of the water and casing, and is evaluated empirically by the observed attenuation of vibrations. The linearized momentum and mass equations may be cross differentiated, resulting in the "telegraph equation" for water hammer

$$\frac{\partial^2 p}{\partial t^2} + \Gamma \frac{\partial p}{\partial t} - c^2 \frac{\partial^2 p}{\partial z^2} = 0 \tag{4a}$$

$$c = \left(\frac{\rho D}{bp_C} + \frac{\rho}{p_W}\right)^{-1/2} \tag{4b}$$

The telegraph equation governs the propagation of electronic signals through a cable, tidal waves through a uniform embayment, vibrations through a rod, and other linearly attenuated, periodic transport phenomena. The water hammer speed c depends in part on the strength and geometry of the casing unlike acoustic waves in the headspace, whose speed rests on ideal gas law parameters [*Street et al.*, 1995].

[6] The water is initially stationary with hydrostatic pressure below a pressurized air/water interface at elevation L (Figure 1)

$$p = p_O + \rho g(L - z) \qquad (t = 0) \tag{5a}$$

$$\frac{\partial p}{\partial t} = 0 \qquad (t = 0) \tag{5b}$$

$$p_O = \rho g(L_E - L) \tag{5c}$$

The pneumatic slug tester establishes the initial headspace pressure p_O, which lowers the static water column below its equilibrium elevation L_E. Equation (2b) relates the initially still water to a zero temporal pressure derivative and implies condition (5b). The pressure at the screen section remains equal to that of the surrounding groundwater, while the upper boundary pressure $p_L(t)$ is set by the pneumatic slug tester at the air/water interface

$$p = \rho g L_E \qquad (z = 0) \tag{6a}$$

$$p = p_L(t) \qquad (z = L) \tag{6b}$$

Equation (6a) holds until the onset of rigid water motion, which exhibits a frequency ω controlled in part by the aquifer permeability. Our water hammer analysis is accordingly valid for small ωt, so that the water hammer frequency must greatly exceed the rigid motion frequency.

2.2. Formal Solution

[7] The LaPlace transform [*Spiegel*, 1965] of equations (4a), (5), and (6) yields a solution for the transformed pressure $\overline{p}$

$$\overline{p} = \frac{\rho g(L_E - z)}{s} + [s\overline{p}_L(s) - p_O]M(s) \tag{7a}$$

$$M(s) = \frac{\sin h\left[\frac{z}{c}\sqrt{s(s+\Gamma)}\right]}{s\sin h\left[\frac{L}{c}\sqrt{s(s+\Gamma)}\right]} \tag{7b}$$

with LaPlace transform variable s and transformed interfacial pressure $\overline{p}_L$ (s). A convolution integral [*Spiegel*, 1965] and the transform pair $M(s)$:$m(t)$ invert equation (7a)

$$p = \rho g(L_E - z) + \int_0^t \frac{dp_L}{d\tau} m(t-\tau)d\tau \tag{8}$$

with convolution time τ. We must find $m(t - \tau)$.

[8] *Carslaw And Jaeger* [1973] suggest that diffusion problems in finite spatial domains have transformed solutions with simple poles similar to $M(s)$. *Hildebrand* [1976] demonstrates that the inverse of a transform composed of simple poles B_N is the sum of the polar residues $Res_{\pm N}$

$$m(t-\tau) = \sum_{N=0}^{\infty} Res_{\pm N}(t-\tau) \tag{9a}$$

$$Res_{\pm N}(t-\tau) = \lim_{s\to B_{\pm N}} (s - B_{\pm N})\exp[s(t-\tau)]M(s) \tag{9b}$$

Each pole generates a zero in the denominator of $M(s)$, so the zeroth pole is zero. The zeroth residue (z/L) is found by using a small argument approximation of the hyperbolic sines in equation (7b). Equations (8) and (9) reduce to

$$p = \rho g L_E\left(1 - \frac{z}{L}\right) + \frac{p_L z}{L} + \sum_{N=1}^{\infty} \Pi_N \tag{10a}$$

$$\Pi_N = \int_0^t \frac{dp_L}{d\tau} Res_{\pm N}(t-\tau)d\tau \tag{10b}$$

with water hammer coefficients Π_N reflecting the interfacial boundary condition. The remaining poles set an argument of $iN\pi$ in the denominator of equation (7b)

$$iN\pi = \frac{L}{c}\sqrt{B_{\pm N}(B_{\pm N} + \Gamma)} \tag{11a}$$

$$B_{\pm N} = \frac{-\Gamma \pm i\Lambda_N}{2} \tag{11b}$$

$$\Lambda_N = \sqrt{\Omega_N^2 - \Gamma^2} \tag{11c}$$

$$\Omega_N = \frac{2N\pi c}{L} \tag{11d}$$

with undamped Ω_N and damped Λ_N frequencies. Figure 2 displays the polar moduli and phases Φ_N

$$B_{\pm N} = \frac{\Omega_N}{2}\exp(\pm i\Phi_N) \tag{12a}$$

$$\Phi_N = \tan^{-1}\left(-\frac{\Lambda_N}{\Gamma}\right) \qquad (\pi/2 < \Phi_N < \pi) \tag{12b}$$

Equation (12b) defines conjugate pairs, and their sum yields a real solution once the residues are computed.

[9] L'Hospital's rule permits us to evaluate the polar residues from equations (7), (9), (11) and (12)

$$Res_{\pm N}(t-\tau) = \frac{(-1)^{N+1}\sin\left(\frac{N\pi z}{L}\right)\exp\left[B_{\pm N}(t-\tau) \mp i\left(\frac{\pi}{2} + \Phi_N\right)\right]}{\pi N\sqrt{1 - \left(\frac{\Gamma}{\Omega_N}\right)^2}} \tag{13}$$

Equations (10b) and (13) specify the water hammer coefficients in integral form

$$\Pi_N(t) = \frac{(-1)^{N+1}\sin\left(\frac{N\pi z}{L}\right)\exp\left[B_{\pm N}t \mp i\left(\frac{\pi}{2} + \Phi_N\right)\right]}{\pi N\sqrt{1 - \left(\frac{\Gamma}{\Omega_N}\right)^2}} \cdot \int_0^t \frac{dp_L}{d\tau}\exp(-B_{\pm N}\tau)d\tau \tag{14}$$

The headspace pressure at the air/water interface sets p_L and accordingly determines Π_N.

2.3. Free Water Hammer Coefficients

[10] We consider a linear opening of the valve over time t_L. Acoustic waves in the headspace add a forcing pressure p_F to the valve function at the air/water interface

$$p_L = p_O\left(1 - \frac{t}{t_L}\right) + p_F(\omega_N) \qquad (t < tL) \tag{15a}$$

$$p_L = p_F(\omega_N) \qquad (t > t_L) \tag{15b}$$

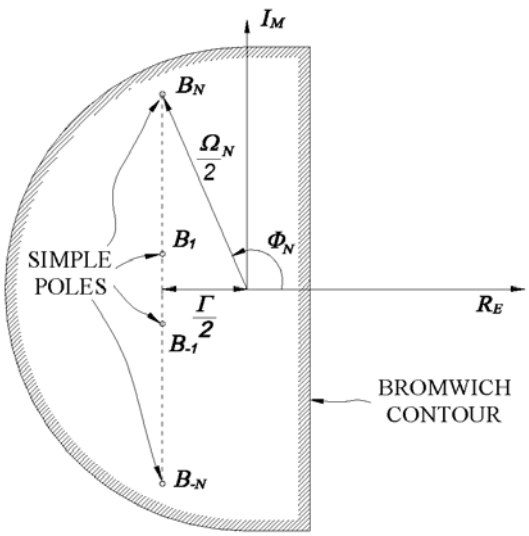

Figure 2. Bromwich contour and simple poles [*Hildebrand*, 1976] for LaPlace transform inversion. Modulus and phase of poles are also shown.

The forcing pressure depends on acoustic wave frequencies ω_N and accordingly forces a frequency response on the water hammer. The valve opening, on the other hand, generates a free response in the water column characterized solely by Ω_N. We pursue the free response by ignoring p_F when equation (15) is substituted into (14). Equations (11), (12), (14), and (15a) specify the free coefficients as the valve opens

$$\Pi_N = \frac{4p_O(-1)^N \sin\left(\frac{N\pi z}{L}\right)}{N\pi\Lambda_N t_L} \cdot \left[\exp\left(-\frac{\Gamma t}{2}\right)\sin\left(\frac{\Lambda_N t}{2} - 2\Phi_N\right) + \sin(2\Phi_N)\right](t < t_L) \tag{16}$$

Equations (11), (12), (14), and (15) specify the free coefficients afterward

$$\Pi_N(t) = \frac{4p_O(-1)^{N+1}\sin\left(\frac{N\pi z}{L}\right)\exp\left(-\frac{\Gamma t}{2}\right)}{N\pi\Lambda_N t_L} \cdot \left\{\exp\left(\frac{\Gamma t_L}{2}\right)\sin\left[\frac{\Lambda_N(t-t_L)}{2} - 2\Phi_N\right] - \sin\left(\frac{\Lambda_N t}{2} - 2\Phi_N\right)\right\} \quad (t > t_L) \tag{17}$$

Equations (11) and (17) suggest that Π_N varies indirectly with $(N\pi)^2 ct_L/L$. We accordingly truncate the series at an N bound by

$$N < \frac{100}{\pi}\sqrt{\frac{L}{ct_L}} \tag{18}$$

Equations (10a), (15a), and (16)–(18) comprise an analytical model of the free (p_F ignored) water hammer in a pneumatic slug test.

2.4. Water Hammer and Rigid, Aquifer-Controlled Motion

[11] The foregoing theory models the progression of water pressure from its initial value (equation (5a)) prior to valve opening to a value prescribed by the first two terms of equation (10a) upon dissipation of the water hammer

$$p \to \rho g L_E\left(1 - \frac{z}{L}\right) \qquad (\Gamma t \to \infty) \tag{19}$$

As the water hammer dissipates, the water column pressure varies linearly from a screen section value ($\rho g L_E$) in equilibrium with the surrounding groundwater to zero at the suppressed air/water interface. The resulting vertical pressure gradient exceeds the weight of the water column by the amount p_O/L, and this excess accelerates the rigid water column as an underdamped slug test. The rigid theory is well established [*Springer and Gelhar*, 1991], and takes equation (19) as an initial condition. *Ostendorf et al.* [2005] derive an expression for the underdamped pressure P in the rigid water column

$$P = -\frac{p_O \exp\left[-\frac{\omega(t-t_L)}{2}\right]}{L_E}\left\{z\cos\left[(t-t_L)\sqrt{\frac{g}{L_E} - \frac{\omega^2}{4}}\right] + [2L_E - z - 2F(L_E - z)]\cdot\frac{\sin\left[(t-t_L)\sqrt{\frac{g}{L_E} - \frac{\omega^2}{4}}\right]}{\sqrt{\frac{4g}{\omega^2 L_E} - 1}}\right\} \quad (\omega t_L \ll 1) \tag{20a}$$

$$F = \frac{f p_O}{8\rho\omega^2 D L_E} \tag{20b}$$

The friction ratio F rests on the Darcy-Weisbach friction factor f and the aquifer controlled ω. The former reflects wall shear stress (external friction) and appreciable fluid velocity (with no vertical gradients) in the column, while aquifer properties and monitoring well geometry provide an order of magnitude estimate of the latter

$$\omega \approx \frac{D^2\mu}{4\rho k L_S L} \tag{21}$$

We note water dynamic viscosity μ and the screen length L_S.

[12] The interaction of water hammer and subsequent rigid fluid motion is approximated by replacing the first

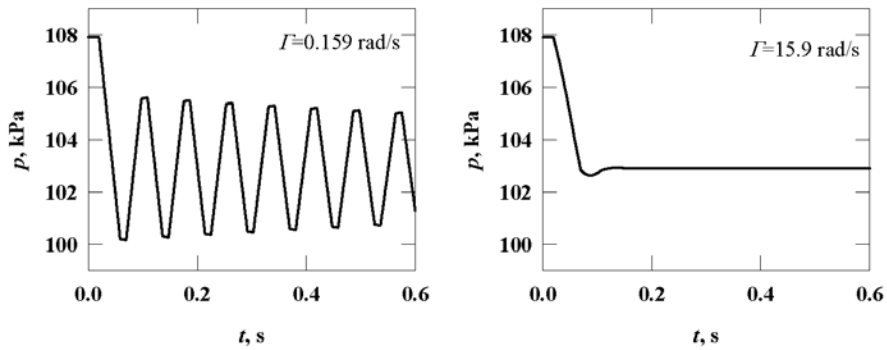

Figure 3. Middepth water hammer simulations for 10 kPa slug test with L = 20 m, z = 10 m, and t_L 0.05 s. Damping coefficient sensitivity: Water hammer persists for weak damping (Γ=0.159 Hz) and dissipates for strong damping (Γ=15.9 Hz).

term in equation (10a) with $P(\omega)$ after the valve opens, so that equations (10a) and (15) become

$$p = \rho g L_E\left(1 - \frac{z}{L}\right) + \frac{p_O z}{L}\left(1 - \frac{t}{t_L}\right) + \sum_{N=1}^{\infty} \Pi_N \quad (t < t_L) \quad (22a)$$

$$p = \rho g (L_E - z) + P(\omega) + \sum_{N=1}^{\infty} \Pi_N \quad (t > t_L) \quad (22b)$$

$$\Omega_1 \gg \omega \quad (22c)$$

$$\Gamma > \omega \quad (22d)$$

The matching of the two models requires a relatively slow aquifer frequency so that ωt is small while water hammer dominates the motion [equation (22c)]. This constraint may be compared to an order of magnitude estimate of Ω_1, obtained by retaining water elasticity only in equations (4b) and (11d). The resulting ratio quantifies our requirement that elastic (water hammer) cycling is much faster than rigid motion (underdamped) periodicity

$$k \gg \frac{D^2 \mu}{8\pi L_S \sqrt{\rho p_W}} \quad (\Omega_1 \gg \omega) \quad (23a)$$

$$k \gg 7 \times 10^{-14} \mathrm{m}^2 \quad (23b)$$

Representative values for μ (10^{-3} kg/m s), D (0.05 m), L_S (1 m), ρ (10^3 kg/m^3), and p_W yield the quantitative constraint (23b). This last is nearly always satisfied for underdamped slug tests, which require relatively permeable soil. Equation (22d) ensures that the water hammer dissipates during the first cycle of the rigid motion, so that equation (19) may serve as an initial condition for the underdamped slug test theory. While the empirical nature of Γ precludes a theoretical estimate of this constraint, the rapid water hammer attenuation observed by *Zurbuchen et al.* [2002], *Zemansky and McElwee* [2005], and *Ostendorf et al.* [2005] all satisfy equation (22d).

3. Simulations and Field Calibration

3.1. Water Hammer Simulations

[13] Figures 3–6 simulate free water hammer propagation induced by a 10 kPa (p_O) pneumatic slug test in schedule

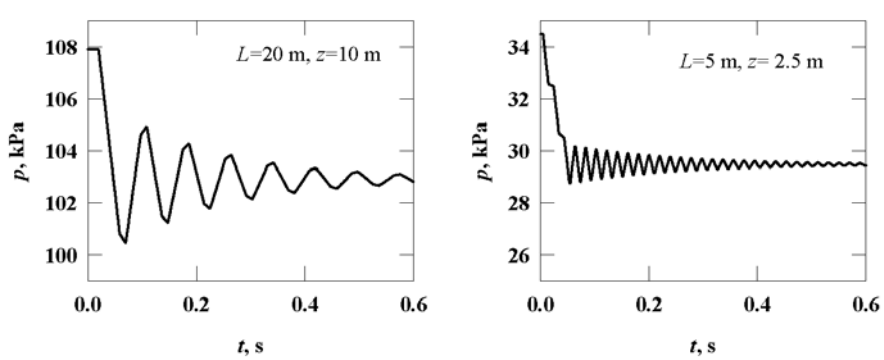

Figure 4. Middepth water hammer simulations for 10 kPa slug test with t_L=0.05 s and Γ=1.59 Hz. Water column length sensitivity: Longer column (L = 20 m) creates water hammer with lower frequency and higher amplitude than shorter column (L = 5 m). Note that dissipation is unaffected by L.

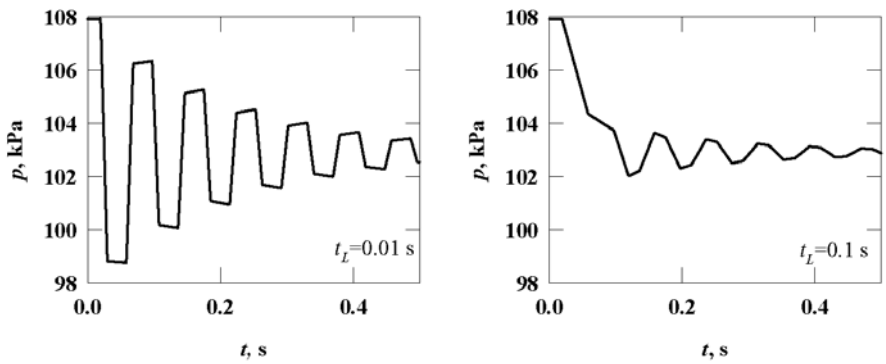

Figure 5. Middepth water hammer simulations for 10 kPa slug test with z = 10 m, L = 20 m, and Γ = 1.59 Hz. Valve closure time sensitivity: Shorter closing time (t_L = 0.01 s) creates higher-amplitude water hammer than longer closing time (t_L = 0.1 s). Dissipation and frequency are unaffected by t_L.

40 PVC casing of nominal 2 inch diameter, which corresponds to D and b values of 5.25 cm and 3.92 mm. The PVC elasticity is taken as 4×10^6 kPa (p_C), representing buried conditions, which strengthen the material property of 2.2×10^6 kPa [*Street et al.*, 1995]. The water compressibility is 2.3×10^6 kPa (p_W). Figure 3 simulates water hammer in a water column length (L) of 20 m, so that the water hammer speed, recalling equation (4b), is 515 m/s and the first undamped water hammer frequency (Ω_1) is 25.8 Hz, by virtue of equation (11d). Figure 3 simulates water hammer at an elevation of 10 m (z) for an opening time of 0.05 s (t_L). Damping coefficients of 0.159 and 15.9 Hz water hammer are run. The water hammer persists for the undamped case (Γ/Ω_1 = 0.006) and disappears for the damped case (Γ/Ω_1 = 0.62).

[14] Figure 4 explores column length sensitivity for Γ equals 1.59 Hz, z middepth, and t_L equals 0.05 s. The water hammer varies strongly with L: the first frequency increases from 25.8 to 103 Hz as the length drops from 20 to 5 m. We accordingly see many more cycles in shorter casing, and the sampling frequency must be high to resolve them. The middepth amplitude is larger in deeper casing as well. Figure 5 simulates sensitivity of water hammer to t_L for a 10 m elevation, a Γ of 1.59 Hz, and an L of 20 m. Rapid opening ($\Omega_1 t_L$ = 1.6) generates larger amplitude water hammer. Gradual opening ($\Omega_1 t_L$ = 16), by contrast, induces more modest water hammer, nearly an order of magnitude

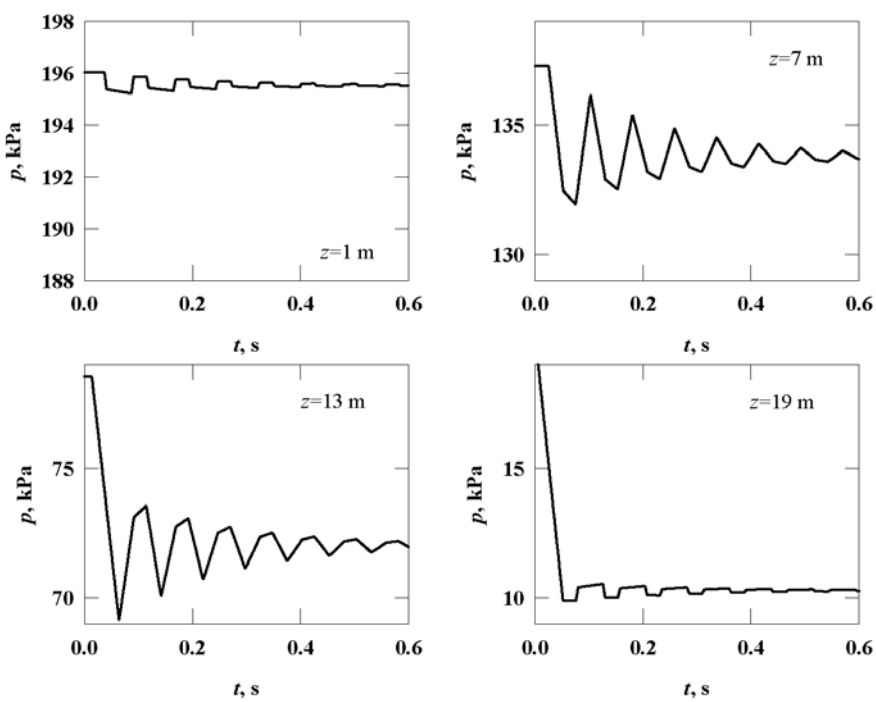

Figure 6. Water hammer simulations for 10 kPa slug test with L = 20 m, Γ = 1.59 Hz, and t_L= 0.05 s. Depth sensitivity: Water hammer is largest near the middle of the water column. Dissipation and frequency are unaffected by z.

Table 1. Prior Slug Test Calibration in Plymouth-Carver Aquifer [a]

z, m	ω, Hz	F
0.95	0.0455	0.096
11.0	0.0519	0.080
19.0	0.0487	0.094

[a]See *Ostendorf et al.* [2005]. Based on 0.31 m amplitude underdamped slug tests conducted in well BO on 29 August 2003.

less in amplitude. The frequencies and attenuation are the same of course, because of common casing length, casing elasticity, and internal friction values for the Figure 5 simulations.

[15] Figure 6 displays depth sensitivity for a 20 m water column with a 0.05 s valve opening time, and a Γ of 1.59 Hz. The water hammer amplitude rises to a maximum in middle of the water column from zero values at each end. The deepest transducer registers a fairly constant pressure near equilibrium (condition (6a)), while the shallowest transducer falls linearly while the valve opens in accordance with the headspace pressure (equations (6b) and (15)).

3.2. Plymouth-Carver Aquifer and kHz Data Acquisition System

[16] We measured water hammer in well BO, made of 5.26 cm diameter (D), schedule 40 PVC of 3.92 mm (b) thickness, and located at a fully characterized field site in the Plymouth-Carver Aquifer [*Ostendorf et al.*, 2005]. The aquifer is a medium sand of high ($\sim 10^{-10}$ m^2) permeability, and well BO had a 1.50 m screen section and an L_E value of 22.4 m. The k value satisfies matching constraint (23b). Table 1 summarizes ω and F values reported by *Ostendorf et al.* [2005], based on 3.04 kPa amplitude slug tests run on August 29, 2003. These data established the validity of equation (20a).

[17] The first inviscid water hammer frequency constrains the sampling frequency $\omega_{\mathrm{SAMPLING}}$ needed to resolve water hammer. Equations (4b) and (11d) govern design of the data acquisition system

$$\omega_{\mathrm{SAMPLING}} \gg \left(L\sqrt{\frac{\rho D}{b p_C} + \frac{\rho}{p_W}} \right)^{-1} (\omega_{\mathrm{SAMPLING}} \gg \Omega_1) \qquad (24)$$

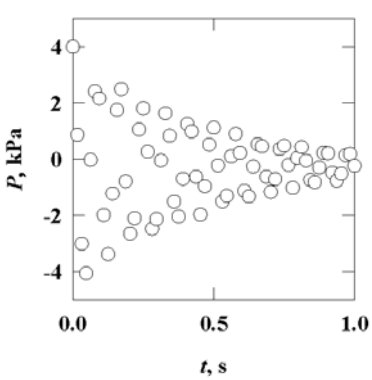

Figure 7. Pressure fluctuations observed at 20 Hz at 11 m elevation in well BO on 23 August 2003 [*Ostendorf et al.*, 2005]. A comparison with Figure 8 suggests that a 20 Hz sampling frequency does not resolve water hammer for this test.

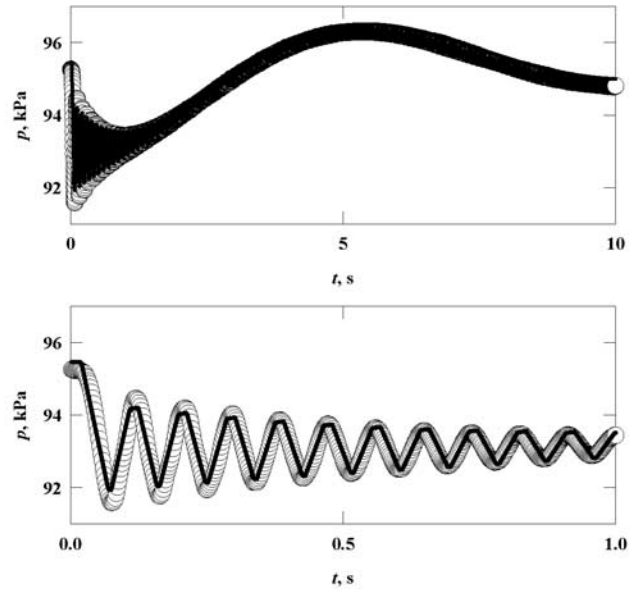

Figure 8. Observed (symbols) and calibrated (curves) pressure, well BO, z = 12.25 m for a 3.97 kPa pneumatic slug test. Well is 5.26 cm diameter, schedule 40 PVC casing, 22 m long, with a 1.50 m screen here and in Figures 9 and 10.

The Plymouth-Carver Aquifer application required a sampling frequency far exceeding the 20 Hz system used in the 2003 experiment conducted at the site. Figure 7, which is abstracted from *Ostendorf et al.* [2005], depicts the aliased

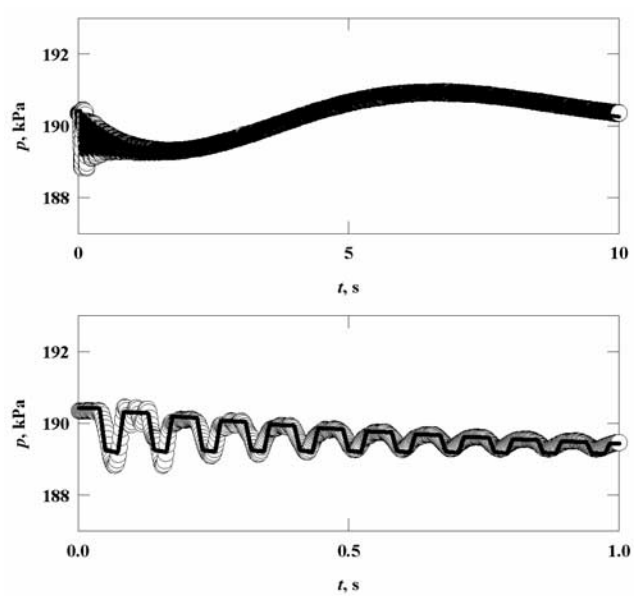

Figure 9. Observed (symbols) and calibrated (curves) pressure, well BO, z = 1.2 m for a 3.97 kPa pneumatic slug test. Note how water hammer dissipates during first seconds, while underdamped slug test persists for over 10 s here and in Figures 8 and 10.

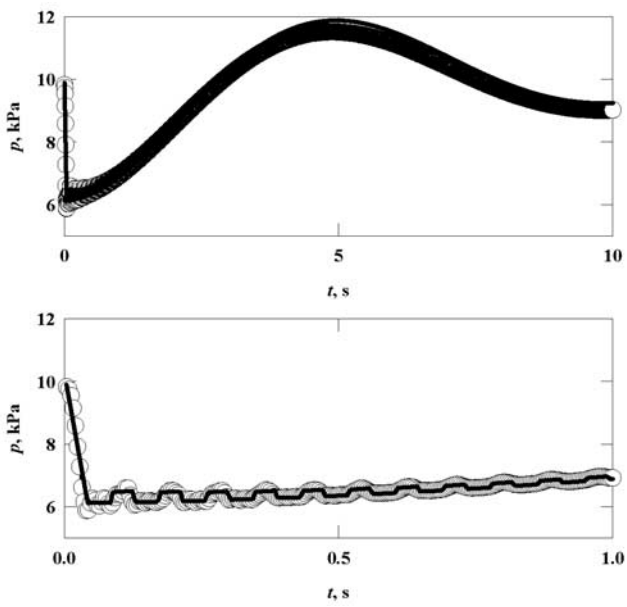

Figure 10. Observed (symbols) and calibrated (curves) pressure, well BO, $z = 19.6$ m for a 3.97 kPa pneumatic slug test. Water hammer disappears before underdamped oscillation begins here and in Figures 8 and 9, confirming the matching constraint of equation (22c). Calibrated k of about 10^{-10} m^2 easily satisfies equation (23b).

results. These data cannot be used to calibrate the water hammer model because they do not resolve the periodicity at the start of the slug test.

[18] Figure 8 displays the properly resolved data under essentially the same conditions, using a kHz data acquisition system [*Dunaj et al.*, 2006], summarized in Figure 1. A 207 kPa pressure transducer (Druck, Fairfield, Connecticut) sensed pressure in the monitoring well. A modular signal conditioning module (National Instruments, Austin, Texas) and a National Instruments PCMCIA 16 bit multifunction I/O analog to digital converter processed the signal at a sampling frequency of 5 kHz, and these data were stored on a laptop computer. The kHz data acquisition system was used with the pneumatic slug tester described by *Ostendorf et al.* [2005].

[19] We ran a series of 3.97 kPa (p_O) pneumatic slug tests in well BO (L = 22.0 m) using the kHz data acquisition system on 23 June 2005, with the results shown as symbols in Figures 8–10. The sampling frequency clearly resolves the superposition of higher-frequency (elastic) and the lower-frequency (rigid) oscillations. The acoustic waves for this test are of relatively high frequency (95.5 Hz) and low amplitude (100 Pa) due to the short (1.5 m) headspace of the experiments. We ignore the acoustic forcing and calibrate the free water hammer waves here. Shallow, middepth, and deep transducer elevations were set in order to document the tendency of water hammer amplitude to increase in middepth of a relatively deep well casing. We adopt the ω and F values of Table 1 for the 2005 well BO calibration, since the newer transducer elevations were close to their 2003 equivalents.

3.3. Field Calibration of Water Hammer Model

[20] We perform a nested Fibonacci search [*Beveridge and Schechter*, 1970] for the t_L, Γ, and p_C values that minimize the root mean square error δ defined by

$$\delta = \sqrt{\sum_{N_T} \frac{[p(\text{measured}) - p(\text{calibrated})]^2}{N_T}} \tag{25}$$

with N_T data points. Table 2 summarizes the calibrations, which are plotted as curves in Figures 8–10. The errors range from 80 to 251 Pa. Since this is 2 to 6% of p_O, the model is reasonably accurate. The calibrated Γ values are consistent, varying from 0.425 to 0.470 Hz, so that water hammer persists over the first few seconds of the slug test. It can accordingly obscure the initial condition for a conventional rigid motion calibration, particularly at middepth (Figure 8). The calibrated damping coefficients in Table 2 all exceed the ω values in Table 1, and satisfy matching constraint (22d).

[21] The calibrated p_C values range from 3.57×10^6 to 3.90×10^6 kPa, all much larger than the literature value of 2.2×10^6 kPa for PVC. This indicates stiffening of the casing by the effective lateral stress of the confining soil around the buried casing. The calibrated water hammer speed [equation (4b)] ranges from 489 to 508 m/s, so that Ω_1 (equation (11d)) is about 22.3 Hz. This damped frequency is two orders of magnitude larger than the rigid aquifer frequencies cited in Table 1, satisfying the matching constraint (22c). Figure 8 makes this point graphically. The damping ratio Γ/Ω_1 is 0.02, so that water hammer persists over 20 to 30 elastic cycles, but dissipates during the first cycle of the underdamped (rigid) motion. The calibrated opening times, which range from 0.034 to 0.055 s, yield an $\Omega_1 t_L$ range of 4.6 to 7.7, which corresponds to fairly slow opening of the valve.

[22] Figures 9 and 10 document the smallness of water hammer near the well screen and the air/water interface, respectively. Figure 9 displays the deep transducer experiment. The relatively small free water hammer amplitude allows the emergence of higher-frequency acoustic wave forcing, which distort the first few cycles of the response. The signal cleans up after a few further cycles however, due to relatively rapid dissipation of the acoustic forcing function. Figure 10 displays a third experiment, conducted near the air/water interface. Here again the water hammer intensity is small, although the pressure drops over the full value of p_O in theory and in fact. Forcing acoustic waves distort

Table 2. Water Hammer Calibration in Plymouth–Carver Aquifer[a]

z, m	p_C, kPa	Γ, Hz	t_L, s	δ, Pa
12.25	3.67×10^6	0.428	0.0548	173
2.55	3.57×10^6	0.470	0.0337	80
20.97	3.90×10^6	0.470	0.0405	251

[a]Based on 0.41 m amplitude underdamped slug tests conducted in well BO on 23 June 2005.

the initial shallow water signal as was the case in deep water. The rigid water motion is most pronounced for the shallowest transducer setting, as measured here and modeled earlier by *Ostendorf et al.* [2005] among others. The present analysis suggests that shallow transducer settings are also less influenced by water hammer, and so are best suited to conventional (rigid motion) calibration, if water hammer is to be ignored.

4. Conclusions

[23] We model and measure the dissipation of relatively high frequency (≈15.9 Hz) water hammer induced by well casing and water elasticity with rapid valve opening at the start of a pneumatic slug test. The water hammer can obscure slower (≈0.159 Hz), aquifer controlled, underdamped oscillations of the rigid water column, so a quantitative description of the elastic motion improves the ability of a slug test to calibrate the aquifer permeability. Internal friction attenuates the water hammer, subject to a known headspace pressure at the air/water interface and equilibrium pressure at the top of the well screen. An analytical free wave solution is presented, with the neglect of water hammer forced by acoustic waves in the headspace. We match the resulting free water hammer model to an existing underdamped analysis, with matching predicated on rapid water hammer dissipation and water hammer frequencies much larger than the slug test frequency. The latter requires that k exceed 7×10^{-14} m^2. The model is consistently calibrated with data from underdamped slug tests at 3 transducer depths in a 22 m deep PVC monitoring well in the Plymouth-Carver Aquifer. The average calibrated p_C of 3.7×10^6 kPa suggests that effective lateral soil stress stiffened the PVC above its unsupported elasticity of 2.2×10^6 kPa. The permeable ($\approx 10^{-10}$ m^2) sand exhibited an underdamped aquifer frequency two orders of magnitude slower than the water hammer, and the average calibrated Γ of 0.462 Hz attenuated the water hammer at the start of rigid water column oscillation. Observed, simulated, and predicted water hammer amplitudes were largest at mid-depth; we may reduce the importance of water hammer by placing the slug test transducer at either end of the water column.

Notation

A casing cross-sectional area (m^2).
B_N Nth simple pole (1/s).
b casing thickness (m).
c water hammer speed (m/s).
D casing internal diameter (m).
F friction ratio.
f Darcy-Weisbach friction factor.
g gravitational acceleration (m/s^2).
k aquifer permeability (m^2).
L pressurized water column length (m).
L_E equilibrium elevation of the air/water interface (m).
L_S screen length (m).
$M(s):m(t)$ LaPlace transform pair.
N_T number of data points.
P underdamped pressure (kg/m s^2).
p gauge pressure (kg/m s^2).
p_C modulus of elasticity of casing (kg/m s^2).
p_F acoustic wave forcing pressure (kg/m s^2).
p_L pressure at air/water interface (kg/m s^2).
p_O initial headspace pressure (kg/m s^2).
p_W bulk modulus of compressibility of water (kg/m s^2).
$\overline{p}$ LaPlace transformed pressure (kg/m s).
$\overline{p_L}$ LaPlace transformed pressure at air/water interface (kg/m s).
Res_N Nth polar residue (1/s).
s LaPlace transform variable (1/s).
t time (s).
t_L time to open valve (s).
w velocity (m/s).
z elevation (m).
δ root mean square calibration error (kg/m s^2).
Γ damping coefficient (Hz).
Λ_N Nth damped water hammer frequency (Hz).
$\Pi_N(t)$ Nth water hammer coefficient (kg/m s^2).
ρ density (kg/m^3).
μ fluid dynamic viscosity (kg/m s).
τ convolution time (s).
Φ_N phase of Nth pole (rad).
Ω_N Nth undamped water hammer frequency (Hz).
ω underdamped slug test frequency (Hz).
ω_N Nth acoustic wave frequency (Hz).
$\Omega_{\mathrm{SAMPLING}}$ sampling frequency (Hz).

[24] **Acknowledgments.** The Massachusetts Highway Department funded this research under interagency service agreement 38721 with the University of Massachusetts at Amherst. The views, opinions, and findings contained in this paper are those of the authors and do not necessarily reflect MassHighway official views or policies. This paper does not constitute a standard, specification, or regulation.

References

Beveridge, G. S. G., and R. S. Schechter (1970), *Optimization: Theory and Practice*, McGraw-Hill, New York.
Bouwer, H., and R. C. Rice (1976), A slug test for determining hydraulic conductivity of unconfined aquifers with completely or partially penetrating wells, *Water Resour. Res.*, *12*(3), 423–428.
Carslaw, H. S., and J. C. Jaeger (1973), *Conduction of Heat in Solids*, Oxford Univ. Press, New York.
Dunaj, P. J., D. J. DeGroot, and D. W. Ostendorf (2006), High frequency data acquisition system for field measurement of hydraulic conductivity in a sand aquifer, paper presented at GeoCongress 2006, Am. Soc. of Civ. Eng., Atlanta, Ga.
Hildebrand, F. B. (1976), *Advanced Calculus for Applications*, Prentice-Hall, Upper Saddle River, N. J.
Hvorslev, M. J. (1951), Time lag and soil permeability in ground water observations, *Waterw. Exp. Stn. Bull. 36*, U. S. Army Corps of Eng., Vicksburg, Miss.
Ostendorf, D. W., D. J. DeGroot, P. J. Dunaj, and J. Jakubowski (2005), A closed form slug test theory for high permeability aquifers, *Ground Water*, *43*(1), 87–101.
Proesser, D. W. (1981), A method of performing response tests on highly permeable aquifers, *Ground Water*, *19*(6), 588–592.
Spiegel, M. R. (1965), *LaPlace Transforms*, McGraw-Hill, New York.
Springer, R. K., and L. W. Gelhar (1991), Characterization of large scale aquifer heterogeneity in glacial outwash by analysis of slug tests with oscillatory responses. Cape Cod, Massachusetts,, *U. S. Geol. Surv. Water Resour. Invest.*, 91–4034.
Street, R. L., G. Z. Watters, and J. K. Vennard (1995), *Elementary Fluid Mechanics*, John Wiley, Hoboken, N. J.
Streeter, V. L., E. B. Wylie, and K. W. Bedford (1998), *Fluid Mechanics*, McGraw-Hill, New York.

van der Kamp, G. (1976), Determining aquifer transmissivity by means of well response tests: The underdamped case, *Water Resour. Res.*, *12*(1), 71–77.

Weaver, W., S. P. Timoshenko, and D. H. Young (1990), *Vibration Problems in Engineering,* John Wiley, Hoboken, N. J.

Zemansky, G. M., and C. D. McElwee (2005), High resolution slug testing, *Ground Water*, *43*(2), 222–230.

Zurbuchen, B. R., V. A. Zlotnik, and J. J. Butler (2002), Dynamic interpretation of slug tests in highly permeable aquifers, *Water Resour. Res.*, *38*(3), 1025, doi:10.1029/2001WR000354.

D. J. DeGroot, P. J. Dunaj, and D. W. Ostendorf, Civil and Environmental Engineering Department, Marston Hall, University of Massachusetts, Amherst, MA 01003, USA. (ostendorf@ ecs.umass.edu)